Characterization of the Local Structures of Ti-MCM-41 and Their Photocatalytic Reactivity for the Decomposition of NO into N_2 and O_2

Yun Hu,[†] Gianmario Martra,[‡] Jinlong Zhang,[§] Shinya Higashimoto,[†] Salvatore Coluccia,[‡] and Masakazu Anpo*,[†]

Department of Applied Chemistry, Graduate School of Engineering, Osaka Prefecture University, 1-1 Gakuen-cho, Sakai, Osaka 599-8531, Japan, Dipartimento di Chimica IFM and NIS Center of Excellence, Università di Torino, Via P. Giuria 7, 10125 Torino, Italy, and Institute of Fine Chemicals, East China University of Science and Technology, Shanghai 200237, P.R. China

Received: August 26, 2005; In Final Form: November 16, 2005

Ti-MCM-41 mesoporous molecular sieves were prepared at ambient temperature and were characterized by X-ray absorption near-edge structure and extended X-ray absorption fine structure, UV−vis, Fourier transform infrared spectroscopy, and photoluminescence spectroscopic analyses. It was found that an increase in the Ti content caused the structure of the Ti-oxides in Ti-MCM-41 to change from an isolated tetrahedral coordination to adjacent Ti-oxide species with Ti^{4+} of tetrahedral coordination. The photocatalytic reactivity of these catalysts for the decomposition of NO into N_2 and O_2 was found to strongly depend on the local structure of the Ti-oxide species including their coordination and distribution, i.e., the charge transfer excited state of the highly dispersed isolated tetrahedrally coordinated Ti-oxides act as the active sites for the photocatalytic decomposition of NO into N_2 and O_2.

1. Introduction

Nitric oxide is an especially harmful atmospheric pollutant and the main cause of acid rain and photochemical smog, which is emitted largely from the reaction of N_2 with O_2 in high-temperature combustion processes. In recent times, the removal of nitrogen oxides (NO_x: NO, N_2O, NO_2), i.e., the direct decomposition of NO_x into N_2 and O_2, has been a great challenge for many researchers.[1−6]

Photocatalysis is an attractive, clean, safe, low-temperature reaction and a nonenergy-intensive approach, especially for for chemical waste remediation. As one of the most popular photoactive catalysts, titanium dioxide has attracted extensive interest due to its various properties such as its nontoxicity, high stability, low cost, and high reactivity for the complete oxidation of a wide variety of organic pollutants and toxic materials into CO_2 and H_2O.[7−10] When the powdered TiO_2 is applied as a photocatalyst for the decomposition of NO in the absence of O_2, it was reported that the formation of N_2O and NO_2 is the major reaction, and the formation of N_2 and O_2 scarcely proceeds.[11,12] On the other hand, highly dispersed titanium oxides prepared in zeolite cavities have been found to exhibit a high and characteristic photocatalytic reactivity for the direct decomposition of NO into N_2 and O_2 as well as the reduction of CO_2 with H_2O into CH_4 and CH_3OH.[12−16] And recently, Ti-containing mesoporous materials such as MCM-41, MCM-48, and HMS have attracted interest as active catalysts for the partial oxidation of alkenes.[17,18] Such systems exhibit the advantage of having a high dispersion of Ti-oxides due to their high internal surface area and nanoscale pore reaction fields. However, there are only a few reports on the photocatalytic reactivity of these materials.[19−21]

In the present work, characterizations of a series of Ti-MCM-41 involving different loadings of Ti-oxides and their photocatalytic reactivities for the direct decomposition of NO into N_2 and O_2 have been investigated by applying various molecular spectroscopic techniques such as photoluminescence, UV−Vis, X-ray absorbtion fine structure (XAFS) (X-ray absorbtion near edge structure [XANES] and Fourier transform extended X-ray absorbtion fine structure [FT-EXAFS]), and Fourier transform infrared spectroscopy (FT-IR). Special attention has been focused on understanding the relationship between the local structures of the Ti^{4+} centers in MCM-41-type materials and their photochemical properties. Moreover, the prepared samples were compared with Ti-HMS mesoporous molecular sieves, which have a thicker pore wall, and also with the TS-1 microporous material to clarify the effect of the support on the photocatalytic reactivity for NO decomposition.

2. Experimental Section

2.1. Catalysts Preparation. MCM-41 and Ti-MCM-41(*X*) (Ti content as wt %: $X = 0.15, 0.60, 0.85, 2.00, 5.00$) were synthesized by following method reported in previous literature using tetraethyl orthosilicate (TEOS) and tetraisopropyl orthotitanate (TPOT) as the starting materials and cetyltrimethylammonium bromide as a structure directing agent.[22] The molar composition of the reaction mixture was 1.0 Si/(0.01−0.10) Ti/0.20 $[C_{16}H_{33}N(CH_3)_3]$ Br/160 H_2O. A high Ti/Si gel ratio was used for this preparation due to the high solubility of Ti under strongly acidic conditions. The reaction mixture was stirred for 5 days at room temperature and then the solid product obtained was filtered, washed, dried, and calcined at 823 K for 6 h with airflow.

Ti-HMS (0.60 wt % as Ti) was prepared from a material mixture having the following composition: 1.0 TEOS/0.0076

* Corresponding author phone, +81-72-254-9282; fax, +81-72-254-9910, e-mail, anpo@chem.osakafu-u.ac.jp.
[†] Osaka Prefecture University.
[‡] Università di Torino.
[§] East China University of Science and Technology.

10.1021/jp058240u CCC: $33.50
Published on Web 01/07/2006

TABLE 1: The Basic Physicochemical Properties of Ti-containing Samples

sample (x)[a]	wt % (solid)	a_o/Å	BET surface area/$m^2\ g^{-1}$
MCM-41	0	37.82	1027
Ti−MCM-41(100)	0.15	38.90	997
Ti−MCM-41(25)	0.60	41.43	915
Ti−MCM-41(14)	0.85	42.05	879
Ti−MCM-41(10)	2.00	44.12	780
Ti−HMS(130)	0.60	58.01	759
TS-1(130)	0.60		457

[a] x = Si/Ti mol ratio in the starting solution.

TPOT/0.2 dodecylamine (DDA)/9.0 EtOH/160 H_2O.[22] TS-1 (0.60 wt % as Ti) was prepared by a hydrothermal synthesis method[23] with a gel mixture of the following ratio: 1.0 TEOS/0.0076 TPOT/0.33 tetrapropylammonium hydroxide (TPAOH)/30 H_2O.

The Ti content in each sample synthesized was determined using atomic absorption method. Prior to spectroscopic measurements and photocatalytic reactions, the catalysts were degassed at 723 K for 1 h and calcined in O_2 (>20 Torr) at 723 K for 2 h, then degassed at 473 K for 2 h.

2.2. Catalyst Characterizations. The powder X-ray diffraction (XRD) patterns of all the samples were recorded on a Shimadzu XD-D1 using Cu K_α radiation (λ = 1.5406 Å). Diffuse reflectance UV−vis spectroscopic measurements were carried out on a Shimadzu UV−vis recording spectrophotometer, UV-2200A. The photoluminescence and lifetimes were measured at 295 K using a Spex 1943D3 spectrofluorophotometer and an apparatus for lifetime measurements, respectively.

The XAFS (XANES and EXAFS) spectra were obtained at the BL-7C facility of the Photon Factory at the National Laboratory for High-Energy Physics, Tsukuba, Japan. The storage ring energy was set at 2.5 GeV and positron current was 260−370 mA. The Ti K-edge absorption spectra were recorded in the fluorescence mode at 295 K. The EXAFS data were examined by an EXAFS analysis program, Rigaku EXAFS. Fourier transform was performed on k^3-weighted EXAFS oscillations in the region of 3−10 $Å^{-1}$ to obtain the radial structure function.

The FT-IR spectra were recorded with a resolution of 4 cm^{-1} at 295 K using a JASCO FT/IR-660 spectrometer. The powdered samples were compressed into thin disk-shaped pellets and mounted in a purpose-made quartz cell attached to a vacuum line similar to that used for photoluminescence in situ analyses.

2.3. Photocatalytic Reactions. The photocatalytic decompositions of NO were performed under a closed system. Typically, 80 mg of the sample was loaded in a quartz cell with a flat bottom (30 mL), which was connected to a vacuum system (10^{-5} Torr range). After pretreatment, NO (180 μmol_Eg-cat.$^{-1}$) was introduced into the quartz cell. UV irradiation of the sample was carried out using a high-pressure mercury lamp (100 W) through a UV cut filter (λ > 240 nm) at 295 K, and a water bath was employed to keep the flat bottom at a constant temperature. The products were analyzed by gas chromatography.

3. Results and Discussion

The powder XRD patterns showed that the Ti-MCM-41 catalysts have a typical hexagonal mesoporous MCM-41 structure. An increase in the *d* spacing or (a_0 values) was observed with an increase in Ti loading for Ti-MCM-41 and the results obtained are shown in Table 1. The increase in the unit cell parameter compared to a siliceous analogue, MCM-41, can be taken as an indication of the incorporation of titanium ions into the framework structure of MCM-41 since the Ti-O bond distance is longer than the Si−O bond distance, and the thickening of the pore wall due to a transition metal promoted a cross-linking of the amorphous silica walls.[22] A similar observation was made of the titanium-incorporated ZSM-5 and HMS frameworks.[17,22,24]

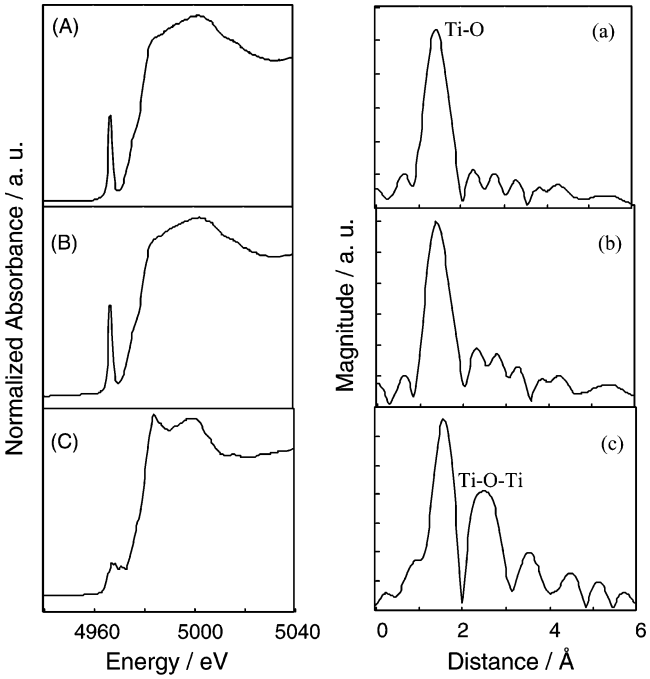

Figure 1. XANES and FT-EXAFS spectra of Ti-MCM-41 with various Ti contents: (A, a) 0.60; (B, b) 2.0; (C, c) 5.0 wt %.

TABLE 2: Curve-fitting Results of FT-EXAFS Data for Ti-MCM-41 and Reference Samples

sample	shell	C. N.[a]	R (Å)[b]	σ^2 ($Å^2$)[c]
Ti−MCM-41(0.6)	Ti−O	3.8	1.80	0.004
Ti−MCM-41(2.0)	Ti−O	4.1	1.81	0.004
Ti−MCM-41(5.0)	Ti−O	5.8	1.93	0.004
$Ti(OPr^i)_4$	Ti−O	4	1.76	0.0009
P-25	Ti−O	6	1.96	0.0009

[a] Coordination number. [b] Bond distance. [c] Debye−Waller factor.

The XANES spectra of the Ti-oxide catalyst at the Ti K-edge show several well-defined pre-edge peaks which are related to the local structure surrounding the Ti atom. Also, the relative intensity of the pre-edge peak provides useful information on the coordination number surrounding the Ti atom. Figure 1 shows the XANES spectra of the Ti-MCM-41 catalysts having various Ti-contents. Ti-MCM-41 (0.6 wt %) and Ti-MCM-41 (2.0 wt %) exhibit an intense single pre-edge peak which can be assigned to the so-called 1s−3d transition, consistent with the tetrahedral coordination for the Ti atoms.[12,25] These two samples show a pre-edge peak of the same intensity and position, indicating that they have the same titanium coordination. On the other hand, Ti-MCM-41(5.0 wt %) shows three characteristic weak pre-edge peaks due to the presence of the crystalline anatase TiO_2 with an octahedral coordination.

Figure 1 also shows the FT-EXAFS spectra of the catalysts while Table 2 shows the results obtained by the curve fitting analysis of the EXAFS spectra. All of the catalysts exhibit a strong peak at around 1.6 Å (without phase shift correction) that can be assigned to the neighboring oxygen atoms (Ti−O). The Ti-MCM-41 (0.6 wt % and 2.0 wt %) catalysts exhibited only a Ti−O peak while Ti-MCM-41 (5.0 wt %) exhibited an additional strong peak at around 2.7 Å due to the

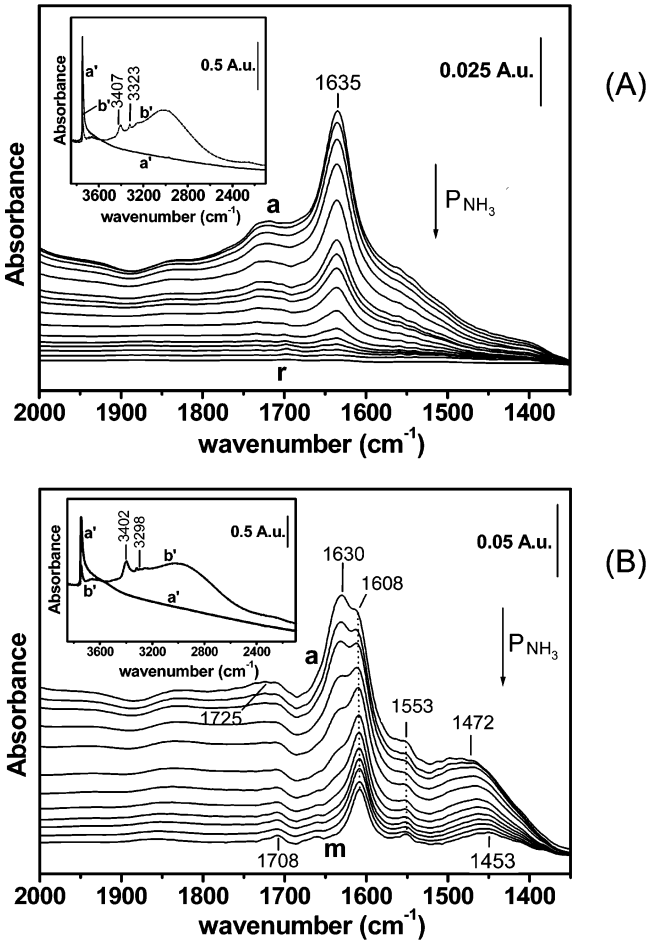

Figure 2. FT-IR spectra of NH_3 molecules adsorbed on: (A) MCM-41 and (B) Ti-MCM-41 (2.0 wt %). The pressure of NH_3 was decreased from 10 Torr to 0 Torr by outgassing at 295 K for 1 min. Inset: (a') Original IR spectra in the high-frequency region of the sample in a vacuum and (b') in the presence of 10 Torr NH_3.

SCHEME 1

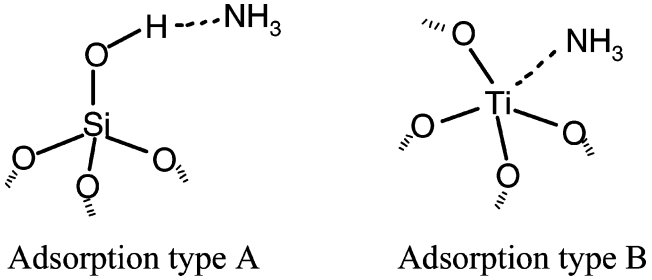

aggregation of the Ti oxide species. The results of the curve-fitting analysis confirmed that even for a Ti content as high as 2.0 wt %, the Ti(IV) centers are located in tetrahedral coordination with four oxygen atoms in the Ti-MCM-41 catalysts.

Ammonia adsorption was used both to monitor the acidity of the surface hydroxyl groups and to elucidate the local environment of the Ti(IV) centers. Figure 2 shows the FT-IR spectra for ammonia adsorption on MCM-41 and Ti-MCM-41 at room temperature. At high NH_3 pressure, a band at 1635 cm^{-1} appeared on the siliceous MCM-41 due to the asymmetric bending mode of the NH_3 molecules adsorbed on the Si−OH groups, while bands at 3407 and 3323 cm^{-1} appeared due to the asymmetric and symmetric stretching vibrations of the adsorbed NH_3, respectively (Scheme 1A).[26,27] Such adsorptions were almost completely reversible at 295 K since all of the IR features associated with the complex completely disappeared

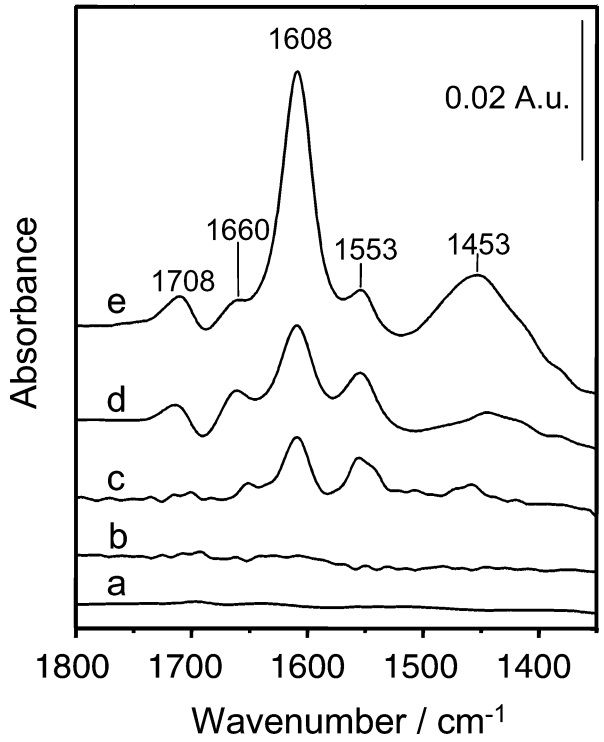

Figure 3. FT-IR spectra of NH_3 molecules adsorbed on MCM-41 (a) and Ti-MCM-41 (b, 0.15; c, 0.60; d, 0.85; e: 2.0 Ti wt %) observed after admission of 10 Torr NH_3 and subsequent outgassing at 295 K for 1 min.

upon outgassing of the samples at 295 K, exhibiting a spectrum similar to that of the bare MCM-41. The complexes formed with NH_3 adsorption on MCM-41 were also formed on Ti-MCM-41 (Figure 2B). Besides these bands, irreversible absorptions at 3402, 3298, and 1608 cm^{-1} assigned, respectively, to the asymmetric stretching, symmetric stretching, and asymmetric bending modes of NH_3 adsorbed on the Ti(IV) Lewis acid sites (Scheme 1B) were observed. The bands at around 1725, 1472, 1660 cm^{-1} can be assigned to the bending modes of NH_4^+ formed by the protonation of the ammonia molecules by the acidic surface hydroxyl groups. The first two bands were observed to shift to 1708 and 1453 cm^{-1}, respectively, after outgassing of the sample at 295 K. The band at 1553 cm^{-1} can be attributed to the Ti−NH_2 or Si−NH_2 bending mode formed by the irreversible reaction of NH_3 with the Si−O−Ti bridges or distorted surface Si−O−Si bridges formed due to the incorporation of Ti into the Si−O−Si networks.[27] Bands for the NH_3 absorbed on Ti-MCM-41 were not observed on TiO_2.

Figure 3 shows the IR spectra resulting from the adsorption of 10 Torr NH_3 on MCM-41 and Ti-MCM-41 (0.15−2.0 wt %), followed by outgassing of the system at 295 K for 1 min. The increase in the Ti content led to an increase in the intensity of this band, indicating that, up to a Ti content of 2.0 wt %, the amount of tetrahedrally coordinated Ti(IV) sites exposed at the surface walls of the channels of the Ti-MCM-41 materials increased with the Ti content.

Nevertheless, as can be seen in Figure 4, the diffuse reflectance UV−Vis spectra exhibited different degrees of dependence on the Ti-loading. In fact, besides a progressive increase in intensity, the increase in the Ti content resulted in a progressive shift of the absorption maximum from 205 to 208 nm [Ti-MCM-41(0.15) and Ti-MCM-41(0.60)] (Figure 4a, b) to 215 nm [Ti-MCM-41(2.0)] (Figure 4d), while a shoulder at ca. 240 nm became evident in the spectrum of Ti-MCM-41(0.85) (Figure 4c), showing a larger contribution in the spectrum of

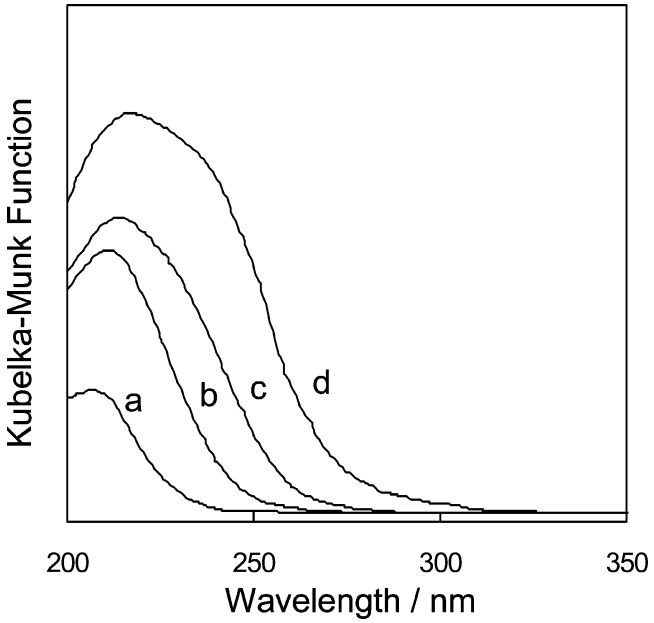

Figure 4. Diffuse reflectance UV−vis spectra of Ti-MCM-41 with different Ti content: (a) 0.15; (b) 0.60; (c) 0.85; and (d) 2.0 wt %.

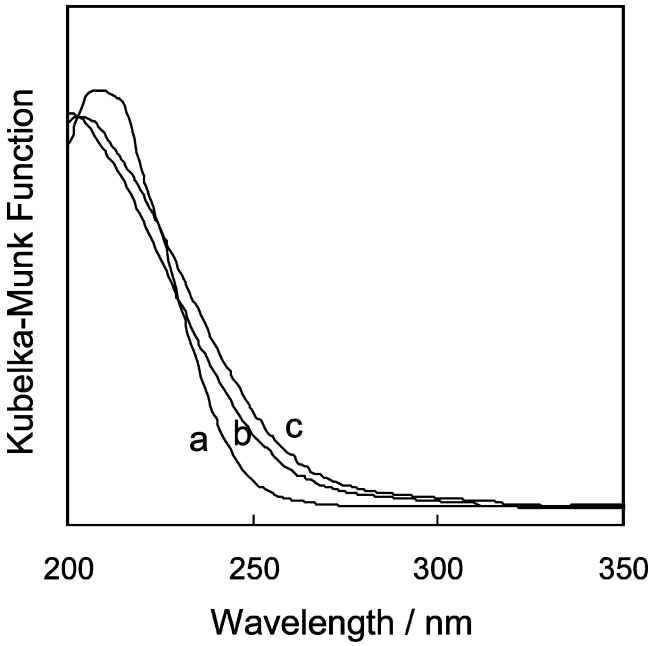

Figure 5. Diffuse reflectance UV−vis spectra of (a) Ti-MCM-41; (b) TS-1; and (c) Ti-HMS (0.6 wt %).

the Ti-MCM-41(2.0) sample by reflecting a larger extent of the Ti-oxide species observed at ca. 250 nm. All the components shown in the absorption ranges are associated with the ligand-to-metal charge transfer processes of the tetrahedrally coordinated Ti-oxide species involving an electron transfer from O^{2-} to Ti^{4+} to form its charge-transfer excited state, $(Ti^{3+}\text{-}O^{-})^*$.[28,29] The absorption bands at 200−210 nm and 220−230 nm are attributed to the isolated tetrahedrally coordinated Ti-oxide species with different framework sites [$Ti(OSi)_4$ and $Ti(OH)(OSi)_3$], while the band at ca. 250 nm is assigned to the tetrahedral titanium dimers or small oligomers.[18,30,31] It should be noted that the band of UV absorption depends not only on the structure but also on the dispersibility of the Ti-oxides. Taking the XAFS results into consideration, it is assumed that the band at 240−250 nm is associated with a decrease in the dispersibility of the isolated tetrahedral Ti-oxides at higher Ti

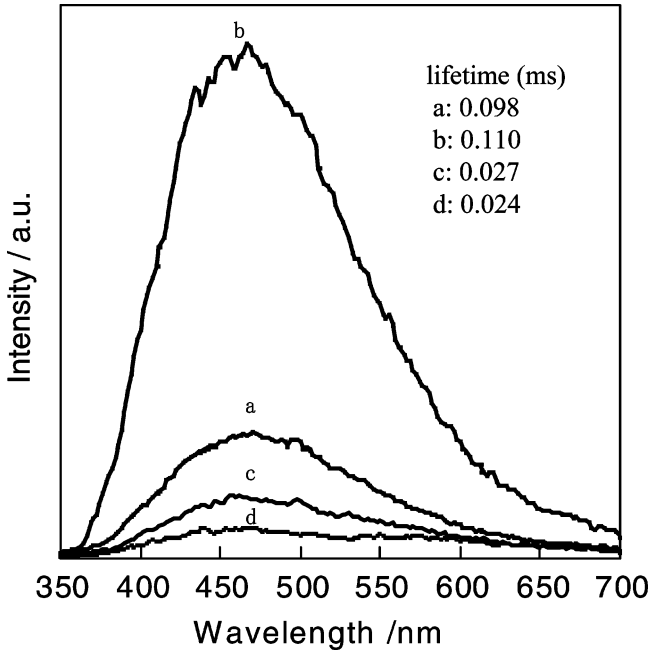

Figure 6. The photoluminescence spectra of Ti-MCM-41 with different Ti content: (a) 0.15; (b) 0.60; (c) 0.85; (d) 2.0 wt %, measured at 295 K.

SCHEME 2

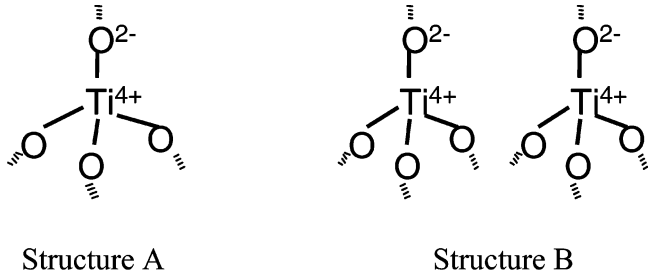

Structure A Structure B

loadings. Ti-HMS and TS-1 shows a similar UV absorption to Ti-MCM-41 centered at around 210 nm, which indicates that the Ti-oxides exist mainly in isolated tetrahedral coordination, as seen in Figure 5. For Ti-HMS and TS-1, the absorption at around 250 nm is slightly more intensive in yield than that of Ti-MCM-41, and this may be due to the lower dispersibility of the isolated tetrahedral Ti-oxides for Ti-HMS and TS-1.

As shown in Figure 6, Ti-MCM-41 exhibits a typical photoluminescence spectrum at around 400−600 nm upon excitation of its charge-transfer band at around 230−260 nm at 295 K, coinciding well with those previously observed for the isolated tetrahedrally coordinated Ti-oxides species highly dispersed in silica matrixes.[32,33] The photoluminescence spectra can be attributed to the reverse radiative decay process from the charge transfer excited triplet to the ground state of the isolated Ti-oxides with a tetrahedral coordination. The intensity of the photoluminescence increased with an increase in the Ti content up to 0.60 wt %, and then sharply decreased with a higher Ti content, as can be seen in Figure 6. Furthermore, it was found that an increase in the Ti content from 0.60 wt % to 0.85 wt % led to a decrease in the phosphorescence lifetime from 0.1 to 0.025 ms. On the basis of these data, when the Ti-MCM-41 materials are photoexcited by UV light, only the isolated tetrahedrally coordinated Ti-oxide species (Scheme 2, A), which are more abundant for Ti contents up to 0.60 wt %, may produce the excited-state long enough to allow the appearance of photoluminescence as a radiative decay to the

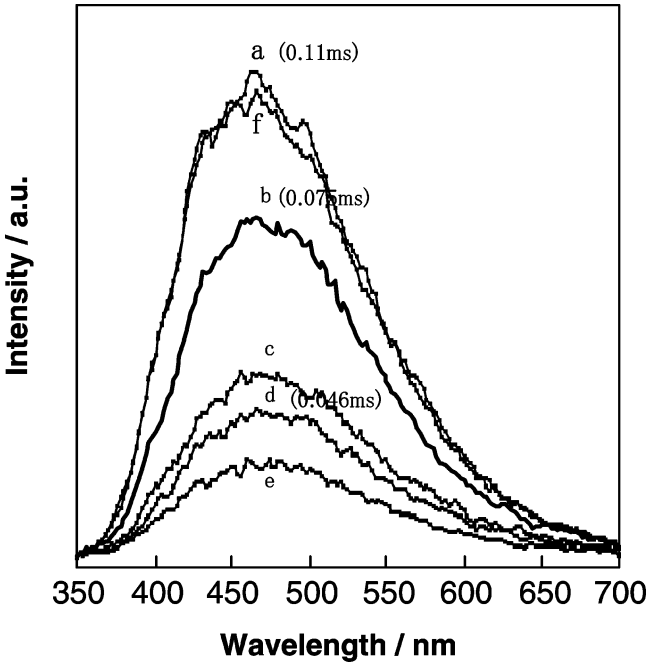

Figure 7. Effect of the addition of NO on the photoluminescence spectra of Ti-MCM-41 (0.60 wt %) measured at 295K. Amount of added NO (in Torr): (a) 0; (b) 0.1; (c) 1.0; (d) 6.0; (e) 20; (f) degassed after (e).

ground state. However, a decrease in the photoluminescence intensity and lifetime for Ti loadings above 0.6 wt % was observed, probably due to the nonradiative deactivation of the photoluminescence arising from an efficient energy transfer to a nearby Ti when the dispersibility of isolated tetrahedral Ti oxide species decrease at higher Ti content. These results suggest that the Ti oxide species exist in different microenvironments from that of highly dispersed isolated tetrahedral coordination. By considering these results, the other structure of the Ti oxide species, different from the isolated tetrahedral species for Ti-MCM-41 which has a high Ti content, can be proposed as Structure B (Scheme 2, B), i.e., the tetrahedral Ti oxide species are adjacent to other Ti-oxide species.

Figure 7 shows that the addition of NO molecules onto the Ti-MCM-41 catalyst leads to an efficient quenching of the photoluminescence as well as a shortening of its lifetime, their extents depending on the amount of added gas, indicating that the added NO molecules interact with the Ti-oxide species in its charge transfer excited triplet state. After degassing of NO at 295 K for 30 min, the photoluminescence recovered to the original intensity level, suggesting that the NO dynamically or collisionally interact with the excited Ti-oxides species.

Figure 8 shows the relationship between the intensity of the $\delta_{asym}NH_3$ band adsorbed on the Ti(IV) centers and the yield of the photoluminescence spectra of Ti-MCM-41 with varying Ti-contents. The intensity of the $\delta_{asym}NH_3$ band (Figure 8a) monitors the total amount of the tetrahedral Ti-oxide species exposed at the surface walls of the Ti-MCM-41 channels, and the yield of the photoluminescence spectrum (Figure 8b) monitors the amount of the isolated tetrahedrally coordinated Ti-oxide species. The yield of the photoluminescence increased with an increase in the Ti content up to 0.6 wt % as well as an increase in the intensity of the NH_3 IR band; however, it decreased with a further increase in Ti content even though the amount of the tetrahedral Ti-oxide species increased. From these results, the Ti-MCM-41 catalyst is proposed to include only an isolated tetrahedral Ti-oxide species with low Ti content while,

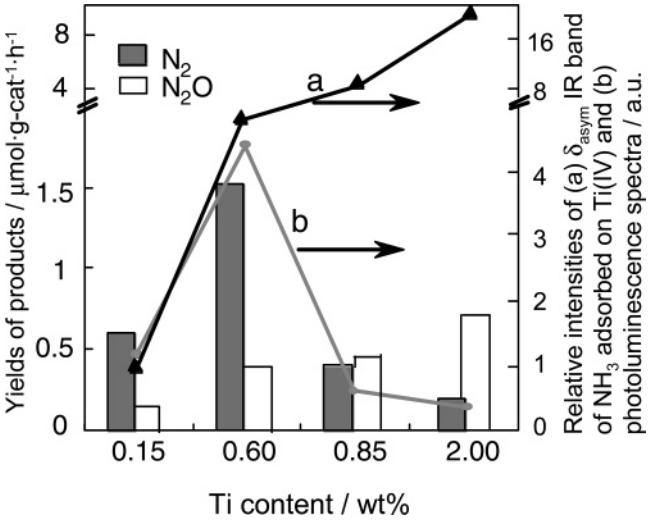

Figure 8. Relationship among the yields of N_2 and N_2O, and the intensities of the IR band of δ asymNH_3 adsorbed on (a) Ti(IV) and (b) photoluminescence spectra of Ti-MCM-41 with various Ti contents.

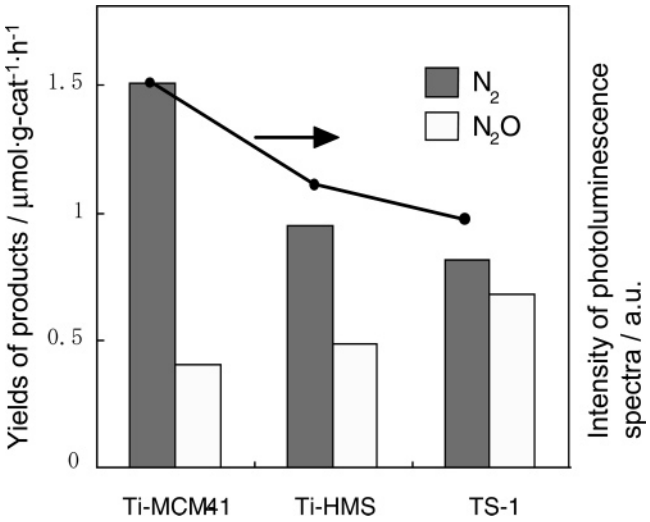

Figure 9. The yields of N_2 and N_2O formation in the photocatalytic decomposition of NO on Ti-MCM-41, Ti-HMS, and TS-1 (0.6 wt %) under UV irradiation at 295 K.

with higher Ti content, the isolated and also adjacent oxides with a tetrahedral Ti-oxide species are included.

UV irradiation of Ti-MCM-41 in the presence of NO was observed to lead to the formation of N_2, O_2, and N_2O at 295 K, their yields increasing in proportion to the irradiation time. No products could be detected either under dark conditions or in UV light irradiation of the siliceous MCM-41. These results clearly indicate that the reaction proceeds photocatalytically on Ti-MCM-41. Figure 8 also shows the effect of the Ti content on the photocatalytic reactivity of the decomposition of NO into N_2 and O_2. The yield and selectivity for the formation of N_2 in the reaction is seen to be the highest for Ti-MCM-41 (0.60 Ti wt %), and an increase in Ti content led to a decrease in the reactivity, showing a good correspondence with the intensities of the photoluminescence spectra due to the isolated tetrahedrally coordinated Ti-oxide species. The amount of the isolated tetrahedrally coordinated Ti-oxide species and not the total amount of the tetrahedral Ti-oxide species exposed at the surface walls of the Ti-MCM-41 channels were, thus, seen to play an important role in the reaction. These results indicate that only the highly dispersed isolated tetrahedrally coordinated Ti-oxide

species acted as the active sites in the photocatalytic decomposition of NO into N_2 and O_2.

The photocatalytic decomposition of NO into N_2 and O_2 proceeded on both Ti-mesoporous and microporous silicate catalysts, as shown in Figure 9. It is clear that the photocatalytic reaction rate and selectivity for the formation of N_2 strongly depended on the type of catalyst. Ti-MCM-41 exhibited much higher activity and selectivity for the formation of N_2 than Ti-HMS and TS-1. It was also found that the yields of N_2 have a good relationship with the intensities of the photoluminescence spectra due to the isolated tetrahedrally coordinated Ti-oxide species. Considering the higher surface area of Ti-MCM-41, the higher activity and selectivity for the formation of N_2 observed for this catalyst may be a contribution of the high dispersion state of the Ti-oxide species.

4. Conclusions

In situ characterizations of Ti-MCM-41 prepared at ambient temperature by combined UV−vis, XAFS, photoluminescence, and FT-IR spectroscopies were seen to be very important in gaining an understanding of the local structures of catalysts with different Ti contents. The local structures of these photocatalysts were found to be very sensitive to the differences in the molecular environment of the reaction field. For catalysts with a Ti content of up to 0.60 wt %, the isolated tetrahedrally coordinated Ti-oxide species existed as the major species, while in catalysts with higher Ti content, the adjacent Ti-oxide species with Ti^{4+} in tetrahedral coordination were seen to be overwhelming in Ti-MCM-41. Their photocatalytic reactivity for the decomposition of NO into N_2 and O_2 was found to strongly depend on the local structure of the Ti-oxide species, i.e., the coordination as well as the dispersibility of the Ti-oxides. The yield and selectivity for the formation of N_2 corresponded well with the yield of the photoluminescence from the charge-transfer excited state of the isolated tetrahedrally coordinated Ti-oxides species, indicating that only these species were involved in the photocatalytic reactions. Ti-MCM-41 showed higher photocatalytic reactivity than Ti-HMS and TS-1 for the decomposition of NO.

Acknowledgment. This work has been supported by a Grant-in-Aid for Scientific Research on Priority Area (#417) from the Ministry of Education, Culture, Sports, Science and Technology (MEXT) of Japan, and M.A. expresses his thanks for their support. Y.H. acknowledges and thanks the Japan Society for the Promotion of Science (JSPS) for their kind financial support.

References and Notes

(1) Notari, B. *Adv. Catal.* **1996**, *41*, 253.
(2) Anpo, M. *Catal. Surv. Jpn. 1* **1997**, 169.
(3) Anpo, M.; Che, M. *Adv. Catal.* **1999**, *44*, 119.
(4) Janssen, F. J. *Handbook of Heterogeneous Catalysis*; Ertl, G., Knozinger, H., Weitkamp, J., Eds.; Wiley-VCH: Weinheim, 1997; Vol. 4, 1633.
(5) Zhang, J.; Ayusawa, T.; Minagawa, M.; Kinugawa, K.; Yamashita, H.; Matsuoka, M.; Anpo, M. *J. Catal.* **2001**, *198*, 1.
(6) Hu, Y.; Zhang, J.; Minagawa, M.; Ayusawa, T.; Matsuoka, M.; Yamashita, H.; Anpo. M. *Res. Chem. Intermed.* **2003**, *29(2)*, 125.
(7) *Photocatalytic Purification and Treatment of Water and Air*; Ollis, D. F., Al-Ekabi, H., Eds.; Elsevier: Amsterdam, 1993.
(8) Anpo, M.; Yamashita, H. *Surface Photochemistry*, Anpo, M., Ed.; Wiley: West Sussex, 1996; p 117.
(9) Hoffmann, M. R.; Martin, S. T.; Choi, W.; Bahnemann, D. W. *Chem. Rev.* **1995**, *95*, 69.
(10) Fan, J.; Yates, J. T. *J. Am. Chem. Soc.* **1996**, *118*, 4686.
(11) Courbon, H.; Pichat, P. *J. Chem. Soc., Faraday Trans. 1* **1984**, *80*, 3175.
(12) Yamashita, H.; Ichihashi, Y.; Anpo, M. *J. Phys. Chem.* **1996**, *100*, 16041.
(13) Zhang, J.; Hu, Y.; Matsuoka, M.; Yamashita, H.; Minagawa, M.; Hidaka, H.; Anpo, M. *J. Phys. Chem. B* **2001**, *105*, 8395.
(14) Anpo, M. *12th International Congress on Catalysis;* Corma, A.; Melo, F. V.; Mendioroz, S.; Fierro, J. L. G., Eds.; Studies in Surface Science and Catalysis, Part A; Elsevier: Amsterdam, 2000; *130*, 157.
(15) Anpo, M.; Higashimoto, S.; Shioya, Y.; Ikeue, K.; Harada, M.; Watanabe, M. *Stud. Surf. Sci. Catal.* **2001**, *140*, 27.
(16) Matsuoka, M.; Anpo, M. *J. Photochem. Photobio. C 3* **2003**, 225.
(17) Blasco, T.; Corma, A.; Navarro, M. T.; Pariente, J. P. *J. Catal.* **1995**, *156*, 65.
(18) Marchese, L.; Gianotti, E.; Dellarocca, V.; Maschmeyer, T.; Rey, F.; Coluccia, S.; Thomas, J. M. *Phys. Chem. Chem. Phys.* **1999**, *1*, 585.
(19) Anpo, M.; Yamashita, H.; Ikeue, K.; Fujii, Y.; Zhang, S. G.; Ichihashi, Y.; Park, D. R.; Suzuki, Y.; Koyamno, K.; Tatsumi, T. *Catal. Today* **1998**, *44*, 327.
(20) Zhang, S. G.; Fujii, Y.; Yamashita, H.; Koyano, K.; Tatsumi, T.; Anpo, M. *Chem. Lett.* **1997**, 659.
(21) Lin, W. Y.; Han, H. X.; Frei, H. *J. Phys. Chem. B.* **2004**, *108*, 18269.
(22) Zhang, W.; Froba, M.; Wang, J.; Tanev, P. T.; Wong, J.; Pinnavaia, T. J. *J. Am. Chem. Soc.* **1996**, *118*, 9164.
(23) Thangaraj. A.; Kumar, R.; Mirajkar, S. P.; Ratnasamy, P. *J. Catal.* **1991**, *130*, 1.
(24) Koningsveld, H.; Jansen, J. C.; Bekkum, H. *Zeolites* **1990**, *10*, 235.
(25) Blasco, T.; Camblor, M. A.; Corma, A.; Perez-Pariente, J. *J. Am. Chem. Soc.* **1993**, *15*, 11806.
(26) Marchese, L.; Gianotti, E.; Maschmeyer, T.; Martra, G.; Coluccia, S.; Thomas, J. M. *Il Nuovo Cimento* **1997**, *19D*, 1707.
(27) Raimondi, M. E.; Gianotti, E.; Marchese, L.; Martra, G.; Maschmeyer, T.; Seddon, J. M.; Coluccia, S. *J. Phys. Chem. B* **2000**, *104*, 7102.
(28) Bordiga, S.; Coluccia, S.; Lamberti, C.; Marchese, L.; Zecchina, A.; Boscherimi, F.; Buffa, F.; Genomi, F.; Leofanti, G.; Petrini, G.; Vlaic, G. *J. Phys. Chem.* **1994**, *98*, 4125.
(29) Prakash, A. M.; Sung-Suh, H. M.; Kaven, L. *J. Phys. Chem. B* **1998**, *102*, 85.
(30) Marchese, L.; Maschmeyer, T.; Gianotti, E.; Coluccia, S.; Thomas, J. M. *J. Phys. Chem. B* **1997**, *101*, 8836.
(31) Ratnasamy, P.; Srinivas, D. *Adv. Catal.* **2004**, *48*, 1.
(32) Anpo, M.; Chiba, K. *J. Mol. Catal.* **1992**, *74*, 207.
(33) Yamashita, H.; Ichihashi, Y.; Harada, M.; Stewart, G.; Fox, M. A.; Anpo, M. *J. Catal.* **1996**, *158*, 97.